34th Annual International Conference of the IEEE EMBS
San Diego, California USA, 28 August - 1 September, 2012

# Compensation for Relative Velocity between Needle and Soft Tissue for Friction Modeling in Needle Insertion

Ali Asadian, Rajni V. Patel, and Mehrdad R. Kermani

*Abstract*— **Percutaneous therapies and in particular needle insertion treatments require an accurate model of needle-tissue interaction. Friction is a major interaction force component during needle insertion, and force-velocity mapping is an indicator of the interaction characteristics. However, soft tissue deformation is an inevitable and complex phenomenon that should be taken into account in order to correct the friction-velocity cycle. The main purpose of this study is to provide a means of compensating for the velocity of tissue with respect to a moving needle in the insertion direction. A high-gain observer is presented which can track this relative motion in a simple manner with no need for computer vision that may pose further challenges. To evaluate the performance of the velocity observer, experiments were carried out on gelatin and agar phantoms.**

## I. INTRODUCTION AND RELATED WORK

Flexible needles have the potential to provide dexterous and precise targeting for percutaneous interventions while reducing the patient's suffering and trauma. However, erroneous needle guidance mitigates the effectiveness of the planned therapy or diagnosis. Much of research on needle insertion has focused on surgical simulation [1], [2], although needle guidance in the contexts of robot-assisted needle insertion has been rapidly growing [3]–[5]. While not fully investigating robustness issues, a significant body of work exists on controlling bevel-tip steerable needles using ideal kinematic models [4], [5]. Accordingly, a steerable needle is controlled from its base through sequential insertion and rotation actions.

The needle itself can be considered as a flexible structure whose shape is determined by needle-tissue interaction forces. Modeling of these forces is challenging, and there has been extensive research work on characterization of the interaction behavior. Using various needle geometries, the complexity and variability of needle response once it is inserted into biological tissues was shown in [6].

Note that the surrounding environment in the needle insertion problem is subject to deformation. Tissue motion is essential in force studies and especially in friction modeling. This is the main focus of the current paper. The approaches reported in the literature for tissue tracking are mostly employed to construct surgical simulators primarily using finite element analysis. Applying this method, X-ray opaque markers were placed at several layers of a silicone gel phantom, and real-time images were captured in indentation tests [2]. Tracking the 2D motion of embedded markers by a CMOS camera, DiMaio and Salcudean [7] modeled force distribution along the needle shaft. Crouch et al. [8] also addressed the velocity-dependency of force profile in transparent silicone gel. In their work, force-displacement data were acquired using multiple layers of fiducial markers whose 3D positions were captured by two digital cameras. Dehghan et al. [9] proposed an experimental technique to build a prostate brachytherapy simulator in which B-mode ultrasound images and radio-frequency (RF) signals were used to measure tissue displacement. In another study to characterize needle-tissue interaction, Hing et al. [10] tracked implanted fiducial beads in tissue using a dual C-arm fluoroscopy. In a different application to model friction, a CCD camera was used to track a single marker attached near the needle-tissue contact point, and then the Karnopp friction model was implemented [11]. In this work, relative inaccuracy and high variance of the estimated parameters can be attributed to the low resolution of the acquired images as well as the camera's low update rate. In an early study on force modeling and identification in needle insertion, Okamura et al. [12] distinguished frictional effects using fluoroscopic images and manual segmentation. However, they did not include tissue displacement in their force model.

The current work is in line with our former studies to find an analytical and feasible representation of needle-tissue interaction and particularly friction. We addressed friction and associated issues in [13] in which tissue motion was not considered due to relative rigidness of the examined sample. However, in clinical procedures, living tissues are expected to deform depending upon the insertion rate and needle type. Thus, soft tissue deformation should be accounted for in friction modeling. Towards this goal, we will analyze tissue motion during needle insertion, and present a functional routine so that our previously developed friction structure [13] can mimic the dynamic nature of translational friction in the presence of tissue deformation.

The rest of this paper is organized as follows. Section II introduces the proposed velocity filtering scheme. Section III presents experimental results, and section IV summarizes the paper with conclusions and suggestions for future work.

## II. ESTIMATION OF TISSUE MOTION FOR RECONSTRUCTING FRICTION-VELOCITY LOOP

We have built this work on our previous friction analysis to deal with significant tissue deformation. Mathematical details

A. Asadian, R.V. Patel, and M.R. Kermani are with Canadian Surgical Technologies and Advanced Robotics (CSTAR), Lawson Health Research Institute, London, ON, N6A 5A5, Canada, and with the Department of Electrical and Computer Engineering, Western University (The University of Western Ontario), London, ON, N6A 5B9, Canada. R.V. Patel is also with the Department of Surgery, Western University (The University of Western Ontario), London, Ontario, Canada (emails: aasadian@uwo.ca, rvpatel@uwo.ca, mkermani@eng.uwo.ca).

978-1-4577-1787-1/12/$26.00 ©2012 IEEE

and the employed procedure regarding the friction model were introduced in [13]. In brief, this LuGre-based scheme is capable of mimicking standard features of the friction phenomenon in solid contacts including viscous friction, hysteresis, and the Stribeck effect. One crucial observation in our extended tests was that this structure could not tolerate tissue deformation, thus was unable to represent the wide hysteresis loop around the origin in the force-velocity cycle. This discrepancy is studied and compensated for in this study.

Note that clinical insertion rates are usually kept low mainly due to safety concerns. One practical issue of applying a low-velocity or low-acceleration profile in feedback control is that ordinary differentiation to compute joint velocities from encoder readings leads to large amounts of computational noise. Thus, to reduce the noise perturbation that can be dominant, a high-gain observer is implemented to estimate the velocity from the encoder measurements. We will benefit from this feature in order to estimate needle-tissue relative motion. Let us denote the joint angle as $\theta$ and the corresponding joint velocity as $\omega$. The estimated values are, therefore, recursively obtained in joint space using (1) in which $i$ and $T$ are respectively the sampling instant and the sampling time [14].

$$\begin{cases} \tilde{\theta}(t_i) = \frac{\epsilon\tilde{\theta}(t_{i-1})+\epsilon T\tilde{\omega}(t_{i-1})+\alpha_1 T\theta(t_i)}{\epsilon+\alpha_1 T} \\ \tilde{\omega}(t_i) = \tilde{\omega}(t_{i-1}) + \frac{\alpha_2 T}{\epsilon}(\theta(t_i) - \tilde{\theta}(t_i)) \end{cases} \quad (1)$$

In (1), $\alpha_1$ and $\alpha_2$ are chosen such that $H(s)$=$s^2 + \alpha_1 s + \alpha_2$ is a Hurwitz polynomial, and $\epsilon$ is set to be 1. In our system, $\tilde{\omega}$ can be replaced with $kv$ where $v$ is the estimated velocity of the robot's distal assembly, and $k$ is a constant value [15]. Thus, using the Z-transform, $V(z)$ is expressed as $V(z)$=$\Psi(z;\alpha_1,\alpha_2)\Theta(z)$ where $\Psi$ is the discrete transfer function of the observer dynamics in (1).

$$\Psi(z;\alpha_1,\alpha_2) = \frac{\alpha_2 T z(z-1)}{(\epsilon+\alpha_1 T)z^2 + (\alpha_2 T^2 - \alpha_1 T - 2\epsilon)z + \epsilon} \quad (2)$$

The following strategy is proposed to be combined with our LuGre-based friction model. This simple technique allows us to formulate translational friction in terms of the insertion rate, and include the effect of relative tissue motion. Note that friction effects in general depend on the relative velocity between moving contacts. That is why applying the LuGre model directly to the insertion force and needle velocity information does not generate an acceptable solution. For example, it cannot represent the existing wide gap around the origin that stems from soft tissue motion. Hence, we require estimation of needle-tissue relative velocity.

Here is the suggested refiltering routine: At first, the original force-velocity loop in terms of $v_f$ is projected to a new space versus $v_s$ using a slow observer. $v_f$ is the outcome of the observation using the vector $\underline{p}_f$=$[\alpha_{1f}, \alpha_{2f}]^T$ that defines a fast observer to track the needle axial motion. $v_s$ also denotes the relative velocity of the moving needle with respect to the deformed tissue. The parameter $\underline{p}_s$=$[\alpha_{1s}, \alpha_{2s}]^T$ defining the slow observer is chosen such that the converted empirical friction-velocity loop in the $v_s$ domain is centered around the origin. The relationship between $v_f$ and $v_s$ is denoted by (3). Note that tuning the second observer requires a few attempts, but it is an easy task. Then, the LuGre-based structure is built based on the transformed force-velocity cycle using $v_s$ and the measured force signals. Finally, the sought force-velocity mapping in the $v_f$ domain is reconstructed taking the inverse Z-transform indicated by (3), and projecting the outcome of the LuGre model to the original force-velocity space.

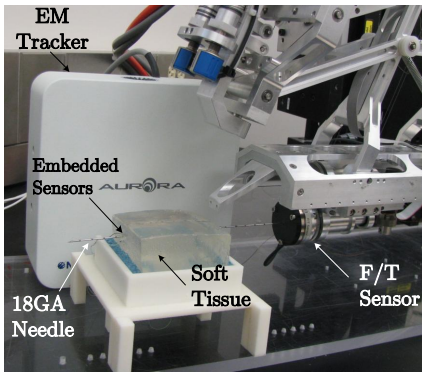


Fig. 1. Our 5-DOF robotic system for needle insertion/steering.

$$\Theta(z) = \frac{V_f(z)}{\Psi(z;\underline{p}_f)} = \frac{V_s(z)}{\Psi(z;\underline{p}_s)} \Rightarrow v_f(t_i) = Z^{-1}\Big\{V_s(z)\frac{\Psi(z;\underline{p}_f)}{\Psi(z;\underline{p}_s)}\Big\} \quad (3)$$

## III. EXPERIMENTAL VALIDATION

### A. Setup Description

An experimental implementation of the proposed approach was carried out on a double parallelogram robotic system fully designed and manufactured in our group for the primary application of prostate brachytherapy [15] (see Fig. 1). This 5-degree-of-freedom (DOF) manipulator can position and rotate the needle body and maintain a Remote Center of Motion (RCM) about its tip.

The robot has been instrumented with a Nano43 6-DOF force/torque sensor (ATI Industrial Automation) to measure the forces/torques acting on the needle shaft. An Aurora electromagnetic tracker (Northern Digital Inc.) is another sensory device that measures the position of its sensor coil(s) with respect to the device's global frame. In our experiments, force data are acquired at the rate of 200Hz while the EM tracker is updated at the rate of 40Hz. Note that the EM tracker is used to evaluate the motion estimation technique.

### B. Experiments and Results

We conducted multiple insertions using a standard 18GA prostate brachytherapy needle (Bard Medical). Validation was performed on the following artificial phantoms: 1) gelatin, 5% concentration, 2) Gelrite Gellan Gum (Sigma-Aldrich), 2% concentration in water. These phantoms simulate an elastic environment. However, gelatin is expected to replicate pure biological tissues better than the Gellan gum since it is an organic artificial material whose main ingredients are bone and skin of pig.

Each tissue sample was placed into a container and clamped such that the bottom of the tissue was rigidly fixed,

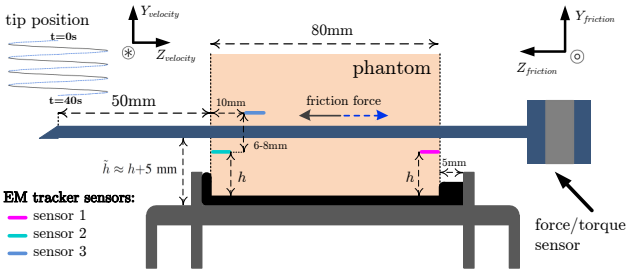


Fig. 2. A schematic of the experimental setup and embedded EM tracker sensors inside soft tissue.

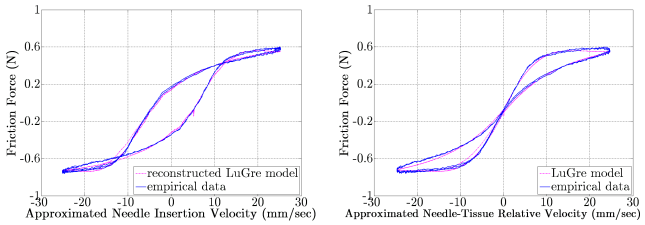


Fig. 3. Experimental and identified friction-velocity cycle with needle-tissue motion compensation in gelatin versus (a) $v_f$ (b) $v_s$ using $\underline{p}_f = [40, 400]^T$ and $\underline{p}_s = [9, 20.25]^T$ ($\tilde{h}$ =50mm).

leaving the sides free to move and unobstructed for needle insertion. Three sensor coils were manually embedded in each phantom at equal vertical distances from the needle shaft (see Fig. 2). In this configuration, sensors 1 and 2 were located very close to the entry and exit points of the needle, and sensor 3 was placed 10mm deeper inside soft tissue compared to sensor 2. The height parameter $\tilde{h}$ was initially adjusted to 50mm, while the phantom was fabricated at the total height of 60mm. A sinusoidal trajectory was applied to insert and withdraw the needle. The amplitude and frequency of this reference signal were set to 40mm and 0.1Hz, respectively; however, this selection was a matter of a few tests to get an initial insight into needle-tissue interaction. The acquired signals were studied over 4 periodic cycles, and using Kalman filtering, the axial velocity of each embedded sensor was extracted from displacement readings. Henceforth, tissue displacements and insertion forces are respectively expressed in the $z$-direction of the tip and the base frames marked by ⊛ and ⊙ signs in Fig. 2. In addition, we assumed for simplicity that both observers were critically damped systems, i.e., $\alpha_{2f}$=$\alpha_{1f}^2/4$ and $\alpha_{2s}$=$\alpha_{1s}^2/4$.

Applying the procedure introduced in section II, the loops shown in Fig. 3 were obtained in gelatin. Initially, by trial and error and setting $\alpha_{1s}$ to 9, the first empirical loop in Fig. 3(a) was transformed to the one in Fig. 3(b). The LuGre friction model was then identified using the converted loop, and the model's output was mapped to the first space afterwards. To validate whether $v_s$ was a good estimate of needle-tissue relative velocity, let us focus on the EM tracker measurements in the next plots. Fig. 4(a) presents the measured tissue displacement at sensor locations, and Fig. 4(b) demonstrates tissue velocity at those points. Repeating the experiments at a number of different insertion points, sensors 2 and 3 reported the minimum and maximum amount of displacement, respectively, while sensor 2 recorded the

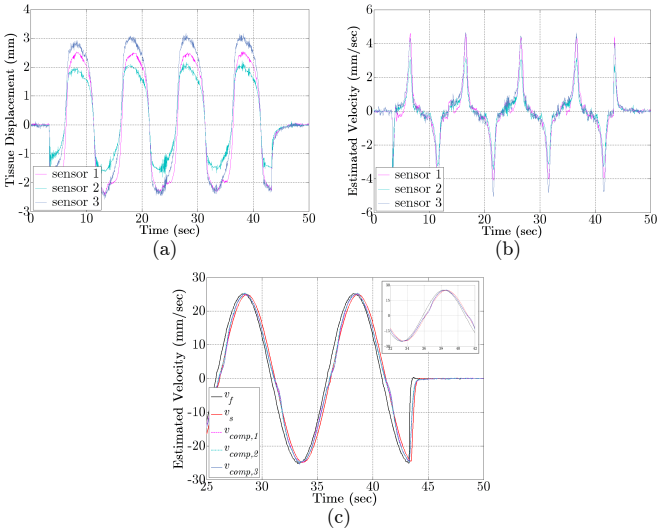


Fig. 4. (a) Relative displacements with respect to initial condition in gelatin (b) estimated tissue axial velocity at sensor locations (c) approximated needle insertion rate and needle-tissue relative velocities extracted from the friction test and sensory measurements ($\tilde{h}$ =50mm).

slowest tissue motion. This observation suggested that soft tissue did not deform uniformly along the insertion path. The next subgraph, Fig. 4(c), displays all velocity components in our problem including needle velocity $v_f$, needle-tissue relative velocity $v_s$ estimated by the tuned slow observer, and needle-tissue relative velocity approximated from EM tracker measurements that could be defined as $v_{comp,i}$=$v_f - v_i$ where $v_i$ is the estimated velocity of each sensor ($1 \leq i \leq 3$). Presented results confirm that there exists a close agreement between $v_s$ and the actual velocities provided by each EM tracker sensor. Throughout our experiments, the best match was found between $v_s$ and $v_{comp,3}$.

In an extended test, insertions were performed at a lower level so $\tilde{h}$ was readjusted to 40mm. As expected, deformation magnitude reduced since the insertion path shifted down towards the firmly fixed edges of tissue container; however, the tracking procedure performed well to capture the needle-tissue relative velocity and frictional effects. Due to the complexity of the trends in general, investigating the practical impacts of incision location and tissue boundary conditions on interaction dynamics will be considered for future work. It is observed in Fig. 2 that tissue attachments at the walls on the both sides of the container are not identical; so it is expected that sensors 1 and 2 would experience different deformations (see Fig. 3(a)).

In the next step, an agar phantom was tested. Due to the rigidity of agar in comparison to gelatin, in this case the sample was only slightly deformed. Thus, as a result of limited measurement accuracy, it was impossible to evaluate the precision of tissue motion estimation using the EM tracker. Nevertheless, the method performed well in practice. Fig. 5 shows the estimated friction in the agar test in which tissue relative motion was compensated by setting $\alpha_{1s}$=22 in the slow observer. As can be seen, the distributed friction was accurately predicted using the proposed mechanism. Due to space limitations, only this graph is included here.

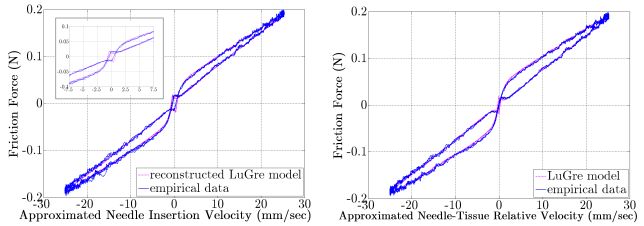


Fig. 5. Experimental and identified friction-velocity cycle with needle-tissue motion compensation in agar versus (a) $v_f$ (b) $v_s$ using $\underline{p}_f = [40, 400]^T$ and $\underline{p}_s = [22, 121]^T$ ($\tilde{h}$ =50mm).

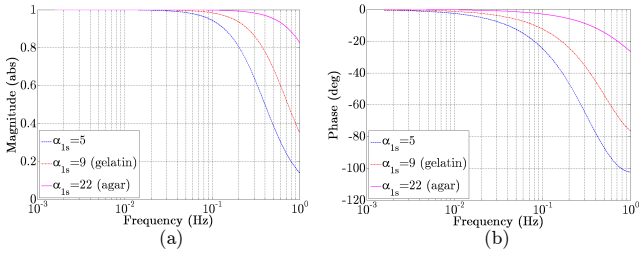


Fig. 6. Bode plots of $H(z)$: (a) magnitude (b) phase.

Finally, to make a frequency-domain analysis, let us revisit $H(z)=\frac{\Psi(z;\underline{p}_s)}{\Psi(z;\underline{p}_f)}$ in (3) where $\underline{p}_f$ was set to $[40, 400]^T$ and $\underline{p}_s=f(\alpha_{1s})$ was subject to change depending on tissue properties. Fig. 6 shows the Bode plots of the transfer function $H$ for three values of $\alpha_{1s}$ parameter. As shown, a smaller $\alpha_{1s}$ value, which is associated with a more deformable soft material, results in a higher amplitude attenuation as well as a greater phase lag with respect to the needle velocity. In this case, at $f_{in}$=0.1Hz (excitation frequency) in gelatin where $\alpha_{1s}$=9, signal attenuation and phase delay were respectively obtained as 1.67% and 12.36°. These quantities for the agar phantom were 0.19% and 2.99°, respectively. Note that based on Fig. 4(c), $v_{comp,3}$ lagged $v_f$ by approximately 10.13°, implying that the key to accounting for tissue motion is to model and later introduce this phase delay into the reference velocity signal as we have done in this study.

## IV. CONCLUSION AND FUTURE WORK

The main advantage of the proposed velocity estimator is its simplicity while preserving accuracy. This velocity observer now in conjunction with our previously developed friction model can accommodate soft-tissue deformation. Thus, the entire scheme is more general and applicable to various needle-tissue combinations without excessive complexity or cost. In our application, no image-based technique was utilized; thus, imaging challenges, e.g., segmentation, artifact minimization, etc. were avoided. Nevertheless, recent advances in Graphic Processing Units (GPUs) have revolutionized computer vision and facilitated fast implementation of complex imaging algorithms.

One possible point to consider for future improvements of the relative-velocity model is to make it adaptive rather than to tune it pre-operatively. Work is also in progress to validate the results via *ex-vivo* experiments using animal organs, e.g., liver, and lung. Ultimately, a full model of friction is expected to be incorporated into motion planners [3]–[5] in order to improve targeting accuracy in clinical practice. Ongoing research by the authors towards this goal is reported in [16] in which only viscous friction was involved to account for needle deflection. On the other hand, surgical simulators are gaining interest in medical and residency training programs. It is very likely that a novice trainee inserts and retracts a needle several times to accomplish a designated task. Thus, inclusion of a bilateral force model with the hysteresis loop which was studied here may enhance haptic perception.

## V. ACKNOWLEDGMENTS

This work was supported by NSERC of Canada under grants RGPIN1345 and RGPIN346166. Financial support for A. Asadian was also provided by an NSERC Collaborative Research and Training Experience (CREATE) program grant #371322-2009 in Computer-Assisted Medical Interventions (CAMI).

## REFERENCES

[1] T.J. Carter, M. Sermesant, D.M. Cash, D.C. Barratt, C. Tanner, and D.J. Hawkes, "Application of Soft Tissue Modelling to Image-Guided Surgery," Med. Eng. Phys., vol. 27, pp. 893-909, 2005.

[2] J. Ma, *et al.*, "Accuracy of Non-linear FE Modelling for Surgical Simulation: Study Using Soft Tissue Phantom," Comp. Biomec. Med., part 1, pp. 29-41, 2010.

[3] A. Haddadi and K. Hashtrudi-Zaad, "Development of a Dynamic Model for Bevel-tip Flexible Needle Insertion into Soft Tissues," In Proc. of 33rd IEEE EMBS Annu. Int. Conf., 2011, pp. 7478-7482.

[4] N.A. Wood, K. Shahrour, M.C. Ost, and C.N. Riviere, "Needle Steering System using Duty-Cycled Rotation for Percutaneous Kidney Access," In Proc. of 32nd IEEE EMBS Annu. Int. Conf., 2010, pp. 5432-5435.

[5] R. Alterovitz, M. Branicky, and K. Goldberg, "Motion Planning Under Uncertainty for Image-Guided Medical Needle Steering," Int. J. Rob. Res., vol. 27, no. 11-12, pp. 1361-1374, 2008.

[6] A. Majewicz, T.R. Wedlick, K.B. Reed, and A.M. Okamura, "Evaluation of Robotic Needle Steering in *ex vivo* Tissue," In Proc. of IEEE Int. Conf. on Rob. Autom. (ICRA), 2010, pp. 2068-2073.

[7] S.P. DiMaio and S.E. Salcudean, "Needle Insertion Modeling and Simulation," IEEE Trans. Robot. and Autom., vol. 19, 2003, pp. 864-875, 2003.

[8] J.R. Crouch, C.M. Schneider, J. Wainer, and A.M. Okamura, "A Velocity-Dependent Model for Needle Insertion in Soft Tissue," In Proc. of MICCAI, 2005, pp. 624-632.

[9] E. Dehghan, X. Wen, R. Zahiri-Azar, M. Marchal, and S.E. Salcudean, "Parameter Identification for a Needle-Tissue Interaction Model," In Proc. of 29th IEEE EMBS Annu. Int. Conf., 2007, pp. 190-193.

[10] J.T. Hing, A.D. Brooks, and J.P. Desai, "A Biplanar Fluoroscopic Approach for the Measurement, Modeling, and Simulation of Needle and Soft-Tissue Interaction," Med. Image Anal., vol. 11, pp. 62-78, 2007.

[11] Y. Kobayashi, T. Sato, and M.G. Fujie, "Modeling of Friction Force based on Relative Velocity between Liver Tissue and Needle for Needle Insertion Simulation," In Proc. of 32nd IEEE EMBS Annu. Int. Conf., 2009, pp. 5274-5278.

[12] A.M. Okamura, C. Simone, and M.D. O'Leary, "Force Modeling for Needle Insertion into Soft Tissue," IEEE Trans. Biomed. Eng., vol. 51, pp. 1707-1716, 2004.

[13] A. Asadian, R.V. Patel, and M.R. Kermani, "A Distributed Model for Needle-Tissue Friction in Percutaneous Interventions," In Proc. of IEEE Int. Conf. on Rob. Autom. (ICRA), 2011, pp. 1896-1901.

[14] H. Khalil, "Adaptive Output Feedback Control of Nonlinear Systems Represented by Input-Output Models," IEEE Trans. Autom. Control, vol. 41, no. 2, pp. 177-188, 1996.

[15] H.S. Bassan, R.V. Patel and M. Moallem, "A Novel Manipulator for Percutaneous Needle Insertion: Design and Experimentation," IEEE/ASME Trans. Mechatron., vol. 14, no. 6, pp. 746-761, 2009.

[16] A. Asadian, M.R. Kermani, and R.V. Patel, "An Analytical Model for Deflection of Flexible Needles During Needle Insertion," In Proc. of IEEE/RSJ Int. Conf. on Intel. Rob. Sys. (IROS), 2011, pp. 2551-2556.